ADVANCED FUNCTIONAL MATERIALS
www.afm-journal.de

Finite-Temperature Properties of Rare-Earth-Substituted $BiFeO_3$ Multiferroic Solid Solutions

Bin Xu, Dawei Wang, Jorge Íñiguez, and Laurent Bellaiche**

Rare-earth substitution in the multiferroic $BiFeO_3$ (BFO) material holds promise for resolving drawbacks inherent to pure BFO, and for enhancing piezoelectric and magneto-electric properties via a control of structural and magnetic characteristics. Rare-earth-doped BFO solid solutions also exhibit unresolved features, such as the precise nature and atomic characteristics of some intermediate phases. Here, an effective Hamiltonian scheme is developed that allows the investigation of finite-temperature properties of these systems from an atomistic point of view. In addition to reproducing experimental results of Nd-doped BFO on structural and magnetic transitions with temperature and composition, this scheme also provides an answer (in form of nanotwins) to these intermediate phases. A striking magneto-electric effect—namely a paramagnetic–to–antiferromagnetic transition that is induced by an applied electric field—is further predicted near critical compositions, with the resulting structural path being dependent on the orientation of the electric field relative to the antiferroelectric vector.

1. Introduction

Multiferroics form an important class of materials that possess coupled long-range-ordered electric and magnetic degrees of freedom.[1] Such magneto-electric coupling is promising to design new devices taking advantage of the control of magnetic properties by the application of an electric field; or conversely, of the magnetic-field-induced change in electric properties. This explains why these fascinating systems have been experiencing a huge regain in interest in the last ten years or so.[2–14] The most studied multiferroic to date is bismuth ferrite ($BiFeO_3$ or BFO) because it exhibits ferroelectricity at a high Curie temperature (T_C = 1100 K) as well as possesses a magnetic ordering (which consists of a G-type based cycloid in the bulk) with a Néel temperature $T_N \approx 640$ K, therefore rendering it a room-temperature multiferroic having a large spontaneous polarization (≈90 μC/cm^2).

However, BFO has several drawbacks, such as large coercive fields and high leakage currents,[15] which can be detrimental for some applications. Such drawbacks can be resolved by alloying BFO with $RFeO_3$ materials for which R is a rare-earth element.[15–18] Doping BFO with rare-earth ion is also known to destroy the magnetic cycloid of BFO in favor of a G-type canted antiferromagnetic structure that allows for the linear magneto-electric effect to occur.[19,20]

Interestingly, recent investigations on the resulting $(Bi_{1-x}R_x)FeO_3$ solid solutions revealed striking behaviors. Examples include the modulated phases observed in the compositional range bridging the well-known ferroelectric *R3c* state (for low *R* concentrations) and the well-determined antipolar *Pnma* phase (for higher *R* compositions). Interestingly, the precise structure and atomic characteristics of these bridging phases are not fully resolved.[15–18,21–23] In particular, the nature and role of oxygen octahedral tiltings and antipolar motions in these phases are subject to debate. Moreover, these bridging phases are further believed to be associated with an enhancement of the piezoelectric responses,[16] whose precise origin remains to be confirmed in our minds. For instance, is it due to the easiness to rotate the polarization in these bridging phases (as similar to the case of the morphotropic phase boundary (MPB) of $Pb(Zr,Ti)O_3$),[24] or rather to the coexistence of different domains involving these bridging phases (which would be consistent with previous works).[22,23] Another example of striking behaviors in $(Bi_{1-x}R_x)FeO_3$ is the strong decrease of the Curie temperature at which the *R3c* state disappears versus the weak dependency of the Néel temperature when increasing the *R* composition, which can therefore lead to the interesting possibility of T_C being equal to T_N (and thus to the optimization of magneto-electricity) for some concentration. Moreover, applying an electric field in the *Pnma* state of *R*-doped BFO systems can lead to an antiferroelectric-to-ferroelectric phase transition (since *Pnma* is antipolar in nature and is close in energy to the ferroelectric *R3c* state in these compounds) that has the potential to be utilized in antiferroelectric capacitors and thus holds promise for energy storage devices.[25]

Dr. B. Xu, Prof. L. Bellaiche
Physics Department and Institute for Nanoscience and Engineering
University of Arkansas
Fayetteville, AK 72701, USA
E-mail: binxu@uark.edu; laurent@uark.edu
Dr. D. Wang
Electronic Materials Research Laboratory-Key Laboratory of the Ministry of Education and International Center for Dielectric Research
Xi'an Jiaotong University
Xi'an 710049, China
Dr. J. Íñiguez
Institut de Ciència de Materials de Barcelona (ICMAB-CSIC)
Campus UAB
08193, Bellaterra, Spain

DOI: 10.1002/adfm.201403811

An atomistic scheme that accurately mimics $(Bi_{1-x}R_x)FeO_3$ solid solutions at finite temperature is therefore highly desirable in order to understand their unusual properties at a microscopic level as well as to guide the design of efficient devices. We are not aware that such scheme exists, likely due to the formidable challenge in treating well the finite-temperature and alloying effects on the subtle magnetic and structural properties of large supercells made of doped BFO compounds.

Here we demonstrate that it is possible to develop such scheme, and apply it to study finite-temperature properties of $Bi_{1-x}Nd_xFeO_3$ (BNFO) as representative of rare-earth-doped BFO systems (note that the choice of R = Nd is also motivated by the fact that numerous measurements have been conducted on this particular system,[16,17,26–28] which will therefore allow us to ground our predictions). Remarkably, this scheme can 1) reproduce very well observed properties, 2) resolve some aforementioned issues, and 3) even predict novel and useful features in this important material.

2. Results and Discussion

2.1. Development of the Numerical Scheme

Practically, we develop an effective Hamiltonian (H_{eff}) approach for BNFO systems. Its degrees of freedom are: 1) the local modes $\{u_i\}$, which are directly related to the local electric dipole centered at the cell i. Note that $\{u_i\}$ are associated with the lowest optical phonon branches, for example, it can correspond to the Gamma point of the Brillouin zone, as in a R3c phase; the X-point antipolar mode, as in a *Pnma* phase[29]; or even more complicated phonons (being neither at the Brillouin zone center nor at the zone border) such as those inherent to nanotwins phases[29,30]; 2) the homogeneous $\{\eta_H\}$ and inhomogeneous $\{\eta_I\}$ strain tensors; 3) the pseudo-vector $\{\omega_i\}$ that characterizes the oxygen octahedral tilting (also termed antiferrodistortive displacement, AFD) about the Fe site i; and 4) the magnetic moment $\{m_i\}$ of the Fe ion located at the site i. Details about this H_{eff}, including the analytical expression of its total energy, are provided in the Experimental Section.

Typical outputs of the simulations[30] are the supercell averages of: 1) the local modes at the Γ and X points, u_Γ and u_X, which are directly proportional to the electrical polarization and the antiferroelectric (AFE) vector associated with the X-point of the cubic first Brillouin zone, respectively; 2) the AFD vectors at the R and M-points, ω_R and ω_M, which characterize the antiphase and in-phase tiltings of the oxygen octahedra, respectively; and 3) the local magnetic moments at the R-point, L, which represents the G-type antiferromagnetic (AFM) vector (note that we did not mimic any magnetic cycloid here because the incorporation of small amount of rare-earth atoms inside BFO is known to annihilate such latter magnetic structure in favor of a G-type AFM arrangement.[19,20]

2.2. Temperature-Induced Phase Transitions

Let us first report the predictions arising from the use of this newly developed H_{eff} for 5%-Nd-doped BFO, as an example. **Figure 1**a shows the variation of the supercell averages of the Cartesian components of the local modes and AFD distortions, and magnitude of the AFM vector L, as a function of temperature for that system. Note that the x-, y-, and z-axis are along the pseudo-cubic [100], [010] and [001] directions, respectively. Below 930 K, the structure is *R3c*, which is characterized by a polarization lying along the pseudo-cubic [111] direction ($u_{\Gamma,x} = u_{\Gamma,y} = u_{\Gamma,z} \neq 0$) and antiphase tilting of the oxygen octahedra about the same pseudo-cubic [111] direction ($\omega_{R,x} = \omega_{R,y} = \omega_{R,z} \neq 0$), while the G-type antiferromagnetic–to–paramagnetic transition occurs at T_N = 655 K (as determined by the inflexion point of $|L|$ in Figure 1a (bottom panel)). Then BNFO with x = 0.05 undergoes transition(s) to complex phase(s) before transforming into the *Pnma* structure at ≈1370 K (note that the *Pnma* phase is characterized

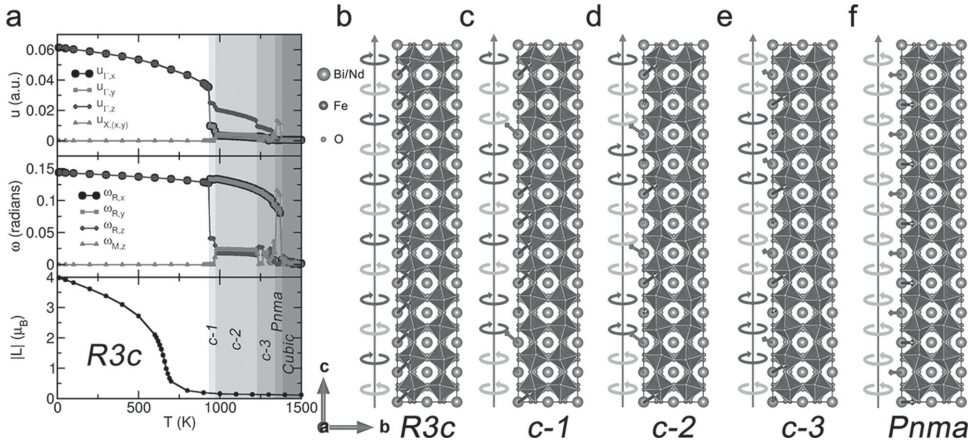

Figure 1. Temperature-induced structural and magnetic phase transitions in disordered $Bi_{0.95}Nd_{0.05}FeO_3$ solid solutions. a) Temperature dependency of the supercell averages of the local modes, u_Γ and u_X, characterizing ferroelectricity and antiferroelectricity, respectively (top), antiphase and in-phase oxygen octahedra tilting vectors, ω_R and ω_M (middle), and the magnitude of the G-type AFM vector in disordered $Bi_{0.95}Nd_{0.05}FeO_3$ solid solutions (bottom). b–f) Structures of the polymorphs appearing in a), viz., b) the low temperature ferroelectric *R3c* phase, c) the first complex phase (c-1), d) the second complex phase (c-2), e) the third complex phase (c-3), and f) the AFE *Pnma* phase. The arrows on the Bi/Nd atoms denote the local dipole vectors with in-plane projection along $[\bar{1}\bar{1}0]$ and [110] pseudo-cubic direction, respectively. The dark and light curled arrows illustrate the clockwise and counterclockwise tilting of the oxygen octahedra along a specific [001] line joining Fe atoms, respectively.

by an antiferroelectric vector pointing along the pseudo-cubic [110] direction, $u_{X,x} = u_{X,y} \neq 0$, antiphase tilting about the [110] direction, $\omega_{R,x} = \omega_{R,y} \neq 0$, and in-phase tilting about the *z*-axis, $\omega_{M,z} \neq 0$). Several complex phases are predicted to exist in BNFO, all possessing an antiphase tilting about the [110] direction and differentiating themselves by the arrangement of the oxygen octahedral tilting about the [001] axis. To characterize such arrangements, we consider a line joining Fe atoms (i.e., the centers of oxygen octahedra) along the [001] direction and denote by *p* and *m* oxygen octahedral tilting in clockwise and counterclockwise fashion, respectively, about the *z*-axis in this line. For instance, we numerically found that three complex structures are present in Figure 1a, which correspond to *mmppmpmppmmp* (between 930 and 960 K), *mmppmmmppmmp* (between 960 and 1220 K) and *mmmppp-mmmppp* (between 1220 and 1320 K). Such structures are schematized in Figure 1c-e, along with *R3c* and *Pnma* shown in Figure 1b and 1f, respectively. These three complex structures can be viewed as intermediate phases between *R3c* and *Pnma*, which are associated with the *pmpm* . . . and *pppp* . . . (or, equivalently, *mmmm* . . .) organization of the oxygen octahedral tilting about [001] along the *z*-axis, respectively (as consistent with their $a^-a^-a^-$ and $a^-a^-c^+$ Glazer notations, respectively).[31] It is worth noting that, as temperature increases, the appearing complex structures tend to possess longer series of in-phase tilting (note also that the existence of these complex tiltings naturally results in the formation of antipolar motions having a longer-than-usual period, which is associated with a k-point that is neither at the center nor at the border of the first Brillouin zone, as demonstrated elsewhere.[29] Their occurrence implies that these nanotwin phases can be thermodynamically (meta)stable and form a family of phases with internal energies ranging between those of *R3c* and *Pnma* for some Nd compositions (comparison of total energies versus composition will be shown later on). They also provide a transition path that possibly involves lower barriers from *R3c* to *Pnma*, as compared to the direct transition between these two states. Figure 1a further shows that the *Pnma* phase is predicted to exist over a very narrow temperature range (e.g., 1350–1370 K for $x = 0.05$), and further heating leads the system to the paraelectric cubic phase (note that melting may occur in reality, before the *Pnma* or *cubic* phase appears, which is not considered in the simulation).

2.3. Compositional Dependency of the Critical Temperatures

Let us now vary the composition of disordered $Bi_{1-x}Nd_xFeO_3$. **Figure 2** shows that the predicted T_N Néel temperature is rather insensitive to the substitution of Bi by Nd ions and the variation of the Nd composition up to $x \approx 0.1625$, as consistent with measurements.[17,26] In fact, the effect of a (small) substitution of Bi by Nd ions is clearly noticeable in the very fast decrease of the transition temperature T_C from *R3c* to the first appearing complex phase when increasing the *x* composition, in rather good agreement with previous observations.[17,26,27] Such different variation of T_N and T_C with the Nd concentration automatically implies that there is a composition for which T_C and T_N should be equal to each other, which is of high relevance for optimizing magneto-electric responses.[32]

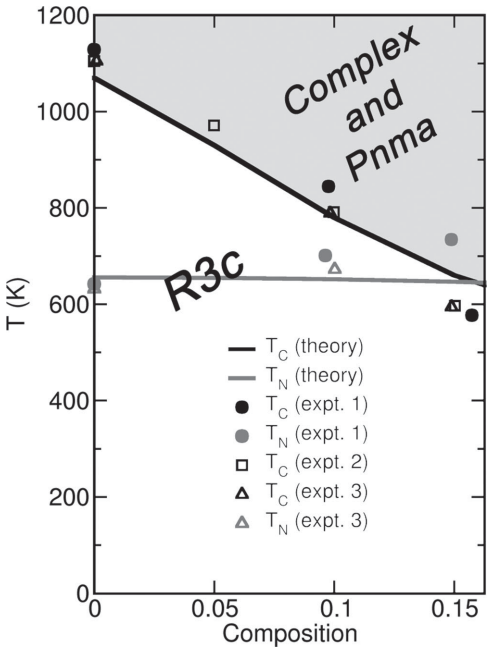

Figure 2. Dependencies of the critical temperatures with composition in disordered $Bi_{1-x}Nd_xFeO_3$ solid solutions. The dark and light lines represent the predicted T_C and T_N, respectively. "expt. 1", "expt. 2" and "expt. 3" refer to the experimental data of other studies.[17,26,27]

Note that, in the compositional range for which *R3c* is found to be experimentally stable from room temperature to ≈700 K (that is, *x* lower than ≈ 0.15),[17] our calculated T_C and T_N are in quantitative agreement with measured values. In particular, our predicted critical composition and temperature when $T_C \approx T_N$, namely $x \approx 0.1625$ and ≈ 640 K, are rather consistent with those that can be extracted from measurements, for example, $x \approx 0.13$ and ≈720 K,[17] and $x \approx 0.13$ and ≈ 680 K[26] (as one can guess from Figure 2, these latter experimental values are only "interpolated" data because of the difficulty in growing different samples with small change in composition). Note, however, that the predictions depicted in Figure 1,2 result from starting the simulations from 10 K adopting a *R3c* phase (that can be easily stabilized by the application of a small electric field along the [111] axis) and progressively heating up the BNFO solid solutions.

2.4. The Effect of Composition on the Ground State

In order to have an idea of what phase is the real ground state for different compositions, **Figure 3** reports the total energies (calculated at 10 K) for four different states, as a function of composition. These states are *R3c*, *Pnma* and two intermediate complex phases (to be denoted by "Complex 1" (*mmppm-mmppmmp*) and "Complex 2" (*mmmpppmmmppp*), as shown in Figure 1c,d, respectively) being representative of the family of nanotwins. With an increasing Nd content *x*, the ground state changes from *R3c* to complex phase(s), and eventually to the *Pnma* phase at around $x \approx 0.34$. The appearance of the complex phases for *x* ranging between 0.06 and 0.34 provides a solution to the intermediate phase(s) experimentally observed in some

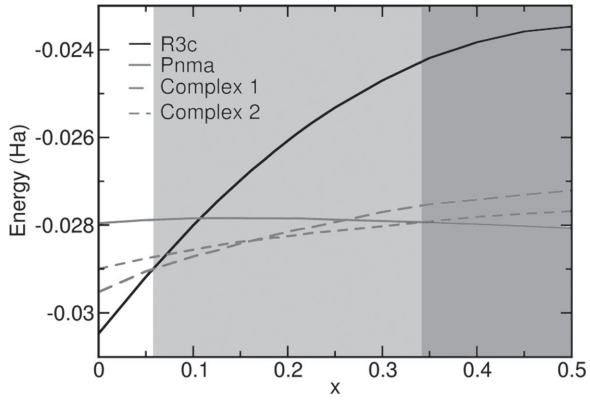

Figure 3. The equilibrium stability of the polymorphs as a function of composition at 10 K. Total internal energies per 5-atom unit cell are calculated for *R3c*, *Pnma* and two intermediate complex phases (denoted as "Complex 1" (*mmppmmmppmmp*, long-dashed line) and "Complex 2" (*mmmpppmmmppp*, short-dashed line)).

compositional window being in-between the region of stabilities of the *R3c* and *Pnma* ground-states.[16,17,21,22] Interestingly, electron diffraction experiment[28] suggested that such intermediate phase may possess an $(a^-a^-c^+)/(a^-a^-c^-)$ tilting pattern, which corresponds to a *ppmm* arrangement of the oxygen octahedral tiltings about [001] along the *z*-axis and which thus belongs to the family of our predicted complex nanotwins.

Moreover, our complex nanotwins also present some antipolar organization (as evidenced by, e.g., the small but nonzero u_X depicted in Figure 1a, which is consistent with the report of antipolar motions from observed diffraction patterns.[16,28] Our prediction that nanotwins can appear in the phase diagram of (Bi,R)FeO_3 is, in fact, in-line with the experimental observation that doped $BiFeO_3$ materials, such as R-doped and Ca-doped $BiFeO_3$, can exhibit nanophasic structures, modulated phases, twin domains and incommensurate modulations.[21–23,33] It is also worthwhile to notice that our model does not require the need to invoke rather complex phenomena (such as flexoelectricity) to explain intermediate phases in $Bi_{1-x}Nd_xFeO_3$ for some compositional range.[23]

Note, however, that determination of the precise tilting arrangement of the intermediate nanotwins, as well as their precise compositional range of stability, in $Bi_{1-x}Nd_xFeO_3$ is a rather difficult challenge for simulations. This is because energy differences between simple phases in pure BFO are already strongly dependent on the functionals used in the ab initio computations[34] and because we numerically found that many different nanotwins can be stable and possess similar energies in $Bi_{1-x}Nd_xFeO_3$ (which is also consistent with the difficulty encountered by experimentalists in determining the exact structure of the intermediate phase(s)). Interestingly, the existence of complex antipolar motions and oxygen octahedral tiltings in these nanotwins, as well as the fact that several of these modulated phases have similar energies, should give rise to striking features in experiments. Examples include superlattice diffraction reflections, characteristic Raman spectra and the possibility that the X-ray diffraction spectra (position and broadening of the peaks) varies in time, as similar to the case of $EuTiO_3$ that is also known to possess a family of nanotwins having low-energy.[35–37]

Furthermore, extrapolating the experimental temperature-versus-composition phase diagram of $Bi_{1-x}Nd_xFeO_3$[17] leads to the transition from an intermediate (complex) phase to *Pnma* for a composition of around 0.30 at low temperature. This is in excellent agreement with the critical composition of 0.34 revealed by Figure 3 for 10 K, which therefore attests the accuracy of our presently developed effective Hamiltonian for mimicking the rather challenging rare-earth-doped BFO materials.

We also numerically found that the *R3c* phase can be quenched to low and intermediate temperatures via, for example, the application of an electric field. Such quenching will allow to check the predictions of Figure 2 that, for compositions close to 16%, *R3c* will not only structurally transform into a complex phase but will also undergo an antiferromagnetic–to-paramagnetic transition, for temperatures close to 640 K.

2.5. Control of the Magnetization with an Electric Field

Note that *Pnma* can also be stabilized at any temperature below, for instance, 1000 K, for the critical composition $x = 0.1625$, since the internal energy of such phase is already close to those of the nanotwins ground states at 10 K and increasing the temperature favors *Pnma* over complex phases (as evidenced by Figure 1 and as consistent with the fact that experiments[16,17] did find *Pnma* phases above ≈600 K for compositions close to 13–17%).

Let us thus investigate a *Pnma* phase for a composition of 16.25% at a temperature of 700 K, that is above the Néel temperature, and consider two different cases corresponding to an electric field, E, oriented along two different directions: a first one along the pseudo-cubic [111] direction versus a second one being parallel to the $[\bar{1}11]$ pseudo-cubic direction. Note that the *Pnma* phase has an AFE vector associated with the *X*-point of the first Brillouin zone, u_X, that lies along the pseudo-cubic [110] direction, implying that the in-plane component of the electric field is parallel to (respectively, perpendicular to) u_X in the first (respectively, second) case. The results for the first and second situations are shown in **Figure 4**a and 4b, respectively.

The top panel of Figure 4a reveals that applying E along [111] and increasing its magnitude first generates a weak polarization along the direction of the electric field that is linear in the strength of E, as typical of AFE systems.[38] Then, $Bi_{0.8375}Nd_{0.1625}FeO_3$ transforms into an intermediate phase (for which the tilting arrangement about the [001] direction is numerically found to be *mppmmppmpppm*) at 7.1×10^8 V/m, followed by the transition to the ferroelectric *R3c* state at 10.4×10^8 V/m. So, once again, the transition from *Pnma* to *R3c* requires the mediation of a nanotwin phase in BNFO systems. What is further remarkable is that this electric-induced path is accompanied by jumps of the magnitude of the AFM vector from a weak (statistically negligible) value in the *Pnma* phase to a large value above 2.3 μ_B in the *R3c* state, via intermediate values ranging between 1.2 and 1.4 μ_B in the nanotwin—see middle panel of Figure 4a. In other words, a remarkable magneto-electric effect consisting of the occurrence of magnetic ordering via the application of an electric field is discovered here (note that we also numerically found (not shown here) that the formation of this AFM is accompanied by the occurrence of

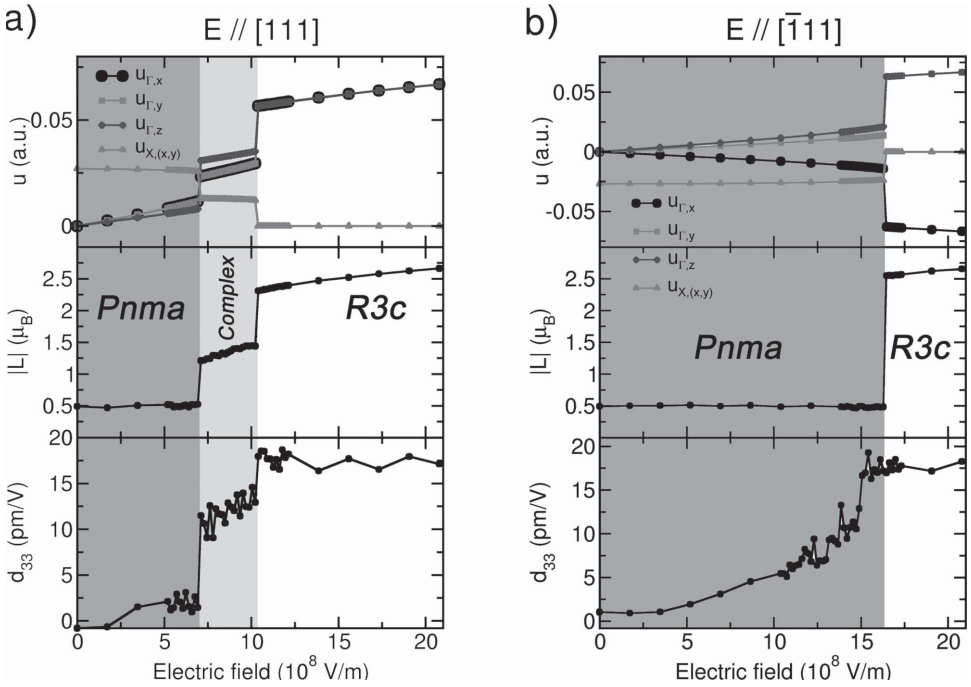

Figure 4. Electric-field induced structural and magnetic transitions in disordered $Bi_{0.8375}Nd_{0.1625}FeO_3$ solid solutions at 700 K. a,b) Electric-field dependency of: the supercell averages of the local modes, u_Γ and u_X, characterizing ferroelectricity and anti-ferroelectricity, respectively (top); the magnitude of the G-type AFM vector (middle); and piezoelectric coefficient d_{33} (bottom). a) Electric field applied along the pseudo-cubic [111] direction; b) Electric field oriented along the pseudo-cubic $[\bar{1}11]$ direction.

a weak magnetization—as consistent with the spin-canted AFM structure known to exist in pure BFO.[39]

Such useful effect originates from the fact that the *R3c* state is naturally antiferromagnetic below 640 K for the composition $x = 0.1625$ (cf. Figure 2), and that an electric field of 10.4×10^8 V/m applied to *Pnma* is able to make the *R3c* state appear at 700 K since *Pnma* and *R3c* are rather close in energy for this composition (see Figure 3). Interestingly, this latter critical field is of the same order than the one recently experimentally applied to BFO films, that is 10^9 V/m.[40] Moreover, the H_{eff} approach has been shown to typically overestimate critical electric fields of BFO-related materials by a factor of 25,[41,42] due to the fact that the calculations consider defect-free systems while grown samples unavoidably possess defects that act as low-energy nucleation centers.[43] As a result, it should be experimentally feasible to check our predictions summarized in Figure 4a.

Regarding the second situation (E along $[\bar{1}11]$), Figure 4b shows that $Bi_{0.8375}Nd_{0.1625}FeO_3$ directly and abruptly transforms from the field-deformed (paramagnetic) *Pnma* phase to the (antiferromagnetic) *R3c* state, that is without the need of any intervening intermediate structure, at a higher critical field of 16.5×10^8 V/m. Such differences in electric-field-driven structural path between Figure 4a,b imply that the orientation of the applied electric field with respect to the AFE vector has a large effect on physical properties, and should be considered when, for example, designing energy-related devices. It is also interesting to realize that the bottom panels of Figure 4a,b demonstrate that the piezoelectric coefficient d_{33} is rather small in the two cases (less than 20 pm/V). Such fact implies that the experimentally observed enhancement of d_{33} at the morphotropic phase boundary of BRFO systems[16] is not due to the structural transition from a pure *Pnma* state to a pure *R3c* but rather originates from a feature that is not presently considered in the computations. As consistent with other studies,[16,21–23] such feature is likely the coexistence of several phases (likely in the form of domains),[44] whose relative occupation fractions depend on the magnitude of the electric field. Note that such coexistence is consistent with the fact that we numerically found (e.g., in Figure 1,3, 4) several stable phases having close energies and with previous first-principles calculations showing that competing and energetically degenerate phases exist in *R*-doped BFO materials.[45]

Note also that the fact that we propose that the piezoelectric response of BRFO can only be enhanced if several phases coexist contrasts with the case of $Pb(Zr_{1-x}Ti_x)\ O_3$ (PZT) solid solutions for which the piezoelectric response can already be large in a single pure phase because of the easiness of rotating the polarization in this phase.[24] Such comparison implies that the MPB of BRFO and PZT differ in nature: one can think of the MPB of BRFO as being discontinuous (as consistent with the abrupt first-order structural changes seen in Figure 4 and as similar to the case of $Bi(Co,Fe)O_3$ materials)[46] while the MPB of PZT can be rather considered to be continuous and second-order-like.

3. Conclusions

It is important to realize (see the Experimental Section) that the main idea behind the development of the proposed

effective Hamiltonian is the effect of chemical pressure arising from the difference in ionic radii between the rare-earth element and Bi^{3+} (and of the lone pair of Bi that makes it more chemically active than *R* ions), on properties of BNFO. As a result, our approach should also be applicable to other BRFO systems, by simply considering the appropriate rare-earth ionic radius in the η_{loc} quantity defined in the Experimental Section. In fact, we did try such approach for $Bi_{1-x}Sm_xFeO_3$ and $Bi_{1-x}Gd_xFeO_3$ (see Supporting Information for details), and were able to qualitatively reproduce the compositional dependency of the critical temperature T_C experimentally found for these systems.[27] In particular, it is interesting to point out that, for a fixed *R* composition, T_C decreases, while T_N increases, when decreasing the ionic radius of the rare-earth element. Such dependencies on the ionic radius provide an additional handle to control the structural, electric and magnetic properties of $(Bi_{1-x}R_x)FeO_3$ systems. We are thus confident that the present development of an effective Hamiltonian approach to treat rare-earth-doped BFO leads to a better understanding of the unusual finite-temperature properties of these fascinating solid solutions, such as resolving the precise nature and atomic characteristics of the intermediate phases experimentally found in some compositional range (see Figure 3) and confirming that, unlike PZT, coexistence of several phases (via domains) is needed to have a large piezoelectric response.[16,21–23] We also hope that all our striking predictions—including the occurrence of a critical (temperature, composition) point for which electrical and magnetic critical temperatures meet (see Figure 2), and the electric-field driven appearance of magnetic ordering (see Figure 4)—will all be experimentally checked soon.

4. Experimental Section

Effective Hamiltonian: As indicated above, we developed an effective Hamiltonian (H_{eff}) approach for BNFO systems having the following degrees of freedom: 1) the local mode $\{u_i\}$ centered on the A site *i* (i.e., on Bi or Nd ions), which are directly related to the local electric dipole centered at the cell *i*; 2) the homogeneous $\{\eta_H\}$ and inhomogeneous $\{\eta_I\}$ strain tensors; 3) the pseudo-vector $\{\omega_i\}$ that characterizes the oxygen octahedral tilting about the Fe site *i*; and 4) the magnetic moment $\{m_i\}$ of the Fe ion located at the site *i*. σ_j (0 or +1) is also introduced to account for the presence of a Bi or Nd ion at the A-lattice site *j*, respectively. We also define a local quantity $\eta_{loc}(i)$ centered on the Fe-site *i* as $\eta_{loc}(i)=\frac{\delta R_{ionic}}{8}\sum_j \sigma_j$, where the sum over *j* runs over the eight A nearest neighbors of eight Fe-site *i* and δR_{ionic} represents the relative difference in ionic radius between Nd and Bi ions. $\eta_{loc}(i)$ is therefore different from zero only if at least one of these eight A sites are occupied by the Nd ions, that is, it vanishes for pure BFO. The total energy of this H_{eff} has two main terms:

$$E_{tot} = E_{BFO}\left(\{u_i\},\{\eta_H\},\{\eta_I\},\{\omega_i\},\{m_i\}\right) + E_{alloy}\left(\{u_i\},\{\omega_i\},\{m_i\},\{\eta_{loc}\}\right) \quad (1)$$

where E_{BFO} is the effective Hamiltonian of pure BFO that has been developed and detailed in previous works.[30,39,47,48] On the other hand, E_{alloy} characterizes the effect of substituting some Bi by Nd ions on physical properties, and is proposed to have the following expression:

$$E_{alloy} = \sum_i \eta_{loc}(i)\left\{\Delta\kappa_u \sum_j u_j^2 + \Delta\kappa_\omega \omega_i^2 + \sum_{k,\alpha,\beta} \Delta J_{ik,\alpha\beta} m_{i,\alpha} m_{k,\alpha} \omega_{i,\beta}^2 + \sum_{j,\alpha,\beta} \Delta D'_{ij,\alpha\beta} \omega_{i,\alpha}\omega_{i,\beta} u_{j,\alpha}\right\} \quad (2)$$

where the sum over *i* runs over all the Fe-sites. The sums over *j* and *k* run over the eight A nearest neighbors and over the six Fe nearest neighbors of the Fe-site *i*, respectively. α and β denotes Cartesian components, with the *x*-, *y*-, and *z*-axis being along the pseudo-cubic [100], [010], and [001] directions, respectively. The fact that E_{alloy} is directly proportional to $\eta_{loc}(i)$ implies that, as consistent with ref. [16], the main assumption of this H_{eff} is that properties of rare-earth-doped systems can be understood by the so-called chemical pressure, that is the ionic radius of the *R* element, in general, and its difference with that of Bi, in particular. $\Delta\kappa_u$ (respectively, $\Delta\kappa\omega$) quantifies how this chemical pressure affect the harmonic energy of the local modes (respectively, AFD motions). Note also the fact that *R* ions are less chemically active than Bi ions, due to their lack of lone pair, is also reflected in the value of $\Delta\kappa_u$. Moreover, $\Delta J_{ik,}\alpha\beta$ characterizes how the effect of oxygen-octahedral-tiltings on magnetic exchange interactions varies when substituting Bi by Nd ions (note that oxygen octahedral tilting are known to play a significant role on magnetic properties of perovskites possessing rare-earth ions.[49–51] Finally, $\Delta D'_{ij,\alpha\beta}$ quantifies how the trilinear coupling between $\omega_{i,}\alpha$, $\omega_{i,}\beta$ and $u_{j,}\alpha$ (which, e.g., induce antipolar motions of the A atoms in a *Pnma* phase[29,30]) is altered by the presence of Nd ions. Note also that this latter alteration is directly responsible for the so-called hybrid improper ferroelectricity.[52–54] Practically, $\Delta\kappa\omega$ and $\Delta D'_{ij,\alpha\beta}$ are extracted by performing first-principles calculations on small supercells. $\Delta\kappa_u$ is also initially obtained by conducting ab initio simulations but is then allowed to vary in order to reproduce the experimental critical T_C temperature of ≈790 K measured in BNFO disordered systems for a Nd composition ≈10%.[26,27] Such variation can be justified by realizing that different functionals used in density functional calculations can yield rather different energetic differences between various polar and antipolar states,[34] which demonstrates the challenge in accurately mimicking properties of BFO and related materials. Finally, $\Delta J_{ik,}\alpha\beta$ is determined by imposing that the Néel temperature of $Bi_{0.9}Nd_{0.1}FeO_3$ is close to the one measured elsewhere,[26,27] that is around 640-670 K. The total energy given in Equation 1 is then used in Monte-Carlo (MC) simulations. Disordered $Bi_{1-x}Nd_xFeO_3$ solid solutions are simulated with a 12 × 12 × 12 supercell (thus containing 8640 atoms), in which a random distribution of Nd atoms is used to generate the alloy structure according to the composition *x*. Most calculations adopted 20 000 MC sweeps for equilibration and an additional 20 000 MC sweeps for calculation of the statistical thermal averages, whereas up to 80 000 MC sweeps were used for equilibration in some critical points (where phase transition occurs) to ensure converged results. Note that the MC simulations naturally result in phases that are dynamically stable because the degrees of freedom of the effective Hamiltonian are allowed to change within these simulations.

Acknowledgements

This work is financially supported by the Department of Energy, Office of Basic Energy Sciences, under contract ER-46612 (B.X. and L.B.) and by NSF Grant No. DMR-1066158 (D.W.). D.W. acknowledges the support from the NSFC grant 51390472 and the 111 Project (B14040). J.I. was financially supported by MINECO-Spain (Grant No. MAT2013-40581-P). The authors are thankful for discussions with Dr. I. Levin, Dr. I. M. Reaney and Dr. Y. Yang. The caption of Figure 1 and typos in the main text were amended on January 27, 2015.

Received: October 30, 2014
Published online: December 2, 2014

[1] G. Catalan, J. F. Scott, *Adv. Mater.* **2009**, *21*, 2463.
[2] T. Zhao, A. Scholl, F. Zavaliche, K. Lee, M. Barry, A. Doran, M. P. Cruz, Y. H. Chu, C. Ederer, N. A. Spaldin, R. R. Das, D. M. Kim, S. H. Baek, C. B. Eom, R. Ramesh, *Nat. Mater.* **2006**, *5*, 823.
[3] D. Lebeugle, D. Colson, A. Forget, M. Viret, A. M. Bataille, A. Gukasov, *Phys. Rev. Lett.* **2008**, *100*, 227602.
[4] R. Haumont, J. Kreisel, P. Bouvier, F. Hippert, *Phys. Rev. B.* **2006**, *73*, 132101.
[5] W. Eerenstein, N. D. Mathur, J. F. Scott, *Nature* **2006**, *442*, 759.
[6] M. Fiebig, T. Lottermoser, D. Fröhlich, A. V. Goltsev, R. V. Pisarev, *Nature* **2002**, *419*, 818.
[7] J. Wang, J. B. Neaton, H. Zheng, V. Nagarajan, S. B. Ogale, B. Liu, D. Viehland, V. Vaithyanathan, D. G. Schlom, U. V. Waghmare, N. A. Spaldin, K. M. Rabe, M. Wuttig, R. Ramesh, *Science* **2003**, *299*, 1719.
[8] N. Hur, S. Park, P. A. Sharma, J. S. Ahn, S. Guha, S. W. Cheong, *Nature* **2004**, *429*, 392.
[9] D. V. Efremov, J. V. Den Brink, D. I. Khomskii, *Nat. Mater.* **2004**, *3*, 853.
[10] T. Lottermoser, T. Lonkai, U. Amann, D. Hohlwein, J. Ihringer, M. Fiebig, *Nature* **2004**, *430*, 541.
[11] H. Zheng, J. Wang, S. E. Lofland, Z. Ma, L. Mohaddes-Ardabili, T. Zhao, L. Salamanca-Riba, S. R. Shinde, S. B. Ogale, F. Bai, D. Viehland, Y. Jia, D. G. Schlom, M. Wuttig, A. Roytburd, R. Ramesh, *Science* **2004**, *303*, 661.
[12] R. J. Zeches, M. D. Rossell, J. X. Zhang, A. J. Hatt, Q. He, C. H. Yang, A. Kumar, C. H. Wang, A. Melville, C. Adamo, G. Sheng, Y. H. Chu, J. F. Ihlefeld, R. Erni, C. Ederer, V. Gopalan, L. Q. Chen, D. G. Schlom, N. A. Spaldin, L. W. Martin, R. Ramesh, *Science* **2009**, *326*, 977.
[13] D. Sando, A. Agbelele, D. Rahmedov, J. Liu, P. Rovillain, C. Toulouse, I. C. Infante, A. P. Pyatakov, S. Fusil, E. Jacquet, C. Carrétéro, C. Deranlot, S. Lisenkov, D. Wang, J.-M. LeBreton, M. Cazayous, A. Sacuto, J. Juraszek, A. K. Zvezdin, L. Bellaiche, B. Dkhil, A. Barthélémy, M. Bibes, *Nat. Mater.* **2013**, *12*, 641.
[14] J. C. Wojdeł, J. Íñiguez, *Phys. Rev. Lett.* **2009**, *103*, 267205.
[15] S. B. Emery, C. J. Cheng, D. Kan, F. J. Rueckert, S. P. Alpay, V. Nagarajan, I. Takeuchi, B. O. Wells, *Appl. Phys. Lett.* **2010**, *97*, 152902.
[16] D. Kan, L. Pálová, V. Anbusathaiah, C. J. Cheng, S. Fujino, V. Nagarajan, K. M. Rabe, I. Takeuchi, *Adv. Funct. Mater.* **2010**, *20*, 1108.
[17] I. Levin, S. Karimi, V. Provenzano, C. L. Dennis, H. Wu, T. P. Comyn, T. J. Stevenson, R. I. Smith, I. M. Reaney, *Phys. Rev. B.* **2010**, *81*, 020103.
[18] W. Chen, W. Ren, L. You, Y. Yang, Z. Chen, Y. Qi, X. Zou, J. Wang, T. Sritharan, P. Yang, L. Bellaiche, L. Chen, *Appl. Phys. Lett.* **2011**, *99*, 222904.
[19] S. T. Zhang, Y. Zhang, M. H. Lu, C. L. Du, Y. F Chen, Z. G. Liu, Y. Y. Zhu, N. B. Ming, X. Q. Pan, *Appl. Phys. Lett.* **2006**, *88*, 162901.
[20] J. A. M. Cagigas, D. S. Candela, E. Baggio-Saitovitch, *J. Phys. Conf. Ser.* **2010**, *200*, 012134.
[21] C.-J. Cheng, D. Kan, S.-H. Lim, W. R. McKenzie, P. R. Munroe, L. G. Salamanca-Riba, R. L. Withers, I. Takeuchi, V. Nagarajan, *Phys. Rev. B.* **2009**, *80*, 014109.
[22] C.-J. Cheng, D. Kan, V. Anbusathaiah, I. Takeuchi, V. Nagarajan, *Appl. Phys. Lett.* **2010**, *97*, 212905.
[23] A. Y. Borisevich, E. A. Eliseev, A. N. Morozovska, C. J. Cheng, J. Y. Lin, Y. H. Chu, D. Kan, I. Takeuchi, V. Nagarajan, S. V. Kalinin, *Nat. Commun.* **2012**, *3*, 775.
[24] L. Bellaiche, A. Garcia, D. Vanderbilt, *Phys. Rev. Lett.* **2000**, *84*, 5427.
[25] X. Tan, C. Ma, J. Frederick, S. Beckman, K. G. Webber, *J. Am. Ceram. Soc.* **2011**, *94*, 4091.
[26] I. Levin, M. G. Tucker, H. Wu, V. Provenzano, C. L. Dennis, S. Karimi, T. Comyn, T. Stevenson, R. I. Smith, I. M. Reaney, *Chem. Mater.* **2011**, *23*, 2166.
[27] S. Karimi, I. M. Reaney, Y. Han, J. Pokorny, I. Sterianou, *J. Mater. Sci.* **2009**, *44*, 5102.
[28] S. Karimi, I. M. Reaney, I. Levin, I. Sterianou, *Appl. Phys. Lett.* **2009**, *94*, 112903.
[29] L. Bellaiche, J. Íñiguez, *Phys. Rev. B.* **2013**, *88*, 014104.
[30] S. Prosandeev, D. Wang, W. Ren, J. Íñiguez, L. Bellaiche, *Adv. Funct. Mater.* **2013**, *23*, 234.
[31] A. M. Glazer, *Acta Crystallogr. Sect. B: Struct. Crystallogr. Crystallogr. Chem.* **1972**, *28*, 3384.
[32] S. Prosandeev, I. A. Kornev, L. Bellaiche, *Phys. Rev. B.* **2011**, *83*, 020102.
[33] C. H. Yang, J. Seidel, S. Y. Kim, P. B. Rossen, P. Yu, M. Gajek, Y. H. Chu, L. W Martin, M. B. Holcomb, Q. He, P. Maksymovych, N. Balke, S. V. Kalinin, A. P. Baddorf, S. R. Basu, M. L. Scullin, R. Ramesh, *Nat. Mater.* **2009**, *8*, 485.
[34] O. Diéguez, O. E. González-Vázquez, J. C. Wojdeł, J. Íñiguez, *Phys. Rev. B.* **2011**, *83*, 094105.
[35] Y. Yang, W. Ren, D. Wang, L. Bellaiche, *Phys. Rev. Lett.* **2012**, *109*, 267602.
[36] M. Allieta, M. Scavini, L. J. Spalek, V. Scagnoli, H. C. Walker, C. Panagopoulos, S. S. Saxena, T. Katsufuji, C. Mazzoli, *Phys. Rev. B.* **2012**, *85*, 184107.
[37] J.-W. Kim, P. Thompson, S. Brown, P. S. Normile, J. A. Schlueter, A. Shkabko, A. Weidenkaff, P. J. Ryan, *Phys. Rev. Lett.* **2013**, *110*, 027201.
[38] B. A. Strukov, A. P. Levanyuk, *Ferroelectric phenomena in crystals: physical foundations*, Springer, Berlin, **1998**.
[39] D. Albrecht, S. Lisenkov, W. Ren, D. Rahmedov, I. A. Kornev, L. Bellaiche, *Phys. Rev. B.* **2010**, *81*, 140401.
[40] H. Yamada, V. Garcia, S. Fusil, S. Boyn, M. Marinova, A. Gloter, S. Xavier, J. Grollier, E. Jacquet, C. Carrétéro, C. Deranlot, M. Bibes, A. Barthélémy, *ACS Nano* **2013**, *7*, 5385.
[41] C. Daumont, W. Ren, I. C. Infante, S. Lisenkov, J. Allibe, C. Carrétéro, S. Fusil, E. Jacquet, T. Bouvet, F. Bouamrane, S. Prosandeev, G. Geneste, B. Dkhil, L. Bellaiche, A. Barthélémy, M. Bibes, *J. Phys. Condens. Matter* **2012**, *24*, 162202.
[42] S. Lisenkov, D. Rahmedov, L. Bellaiche, *Phys. Rev. Lett.* **2009**, *103*, 047204.
[43] R. Landauer, *J. Appl. Phys.* **1957**, *28*, 227.
[44] S. Fujino, M. Murakami, V. Anbusathaiah, S. H. Lim, V. Nagarajan, C. J. Fennie, M. Wuttig, L. Salamanca-Riba, I. Takeuchi, *Appl. Phys. Lett.* **2008**, *92*, 202904.
[45] O. E. González-Vázquez, J. C. Wojdeł, O. Diéguez, J. Íñiguez, *Phys. Rev. B.* **2012**, *85*, 064119.
[46] O. Diéguez, J. Íñiguez, *Phys. Rev. Lett.* **2011**, *107*, 057601.
[47] I. A. Kornev, S. Lisenkov, R. Haumont, B. Dkhil, L. Bellaiche, *Phys. Rev. Lett.* **2007**, *99*, 227602.
[48] S. Lisenkov, I. A. Kornev, L. Bellaiche, *Phys. Rev. B.* **2009**, *79*, 012101.
[49] H. J. Zhao, W. Ren, X. M. Chen, L. Bellaiche, *J. Phys. Condens. Matter* **2013**, *25*, 385604.
[50] H. J. Zhao, W. Ren, Y. Yang, X. M. Chen, L. Bellaiche, *J. Phys. Condens. Matter* **2013**, *25*, 466002.
[51] H. J. Zhao, W. Ren, Y. Yang, J. Íñiguez, X. M. Chen, L. Bellaiche, *Nat. Commun.* **2014**, *5*, 4021.
[52] N. A. Benedek, C. J. Fennie, *Phys. Rev. Lett.* **2011**, *106*, 107204.
[53] J. M. Rondinelli, C. J. Fennie, *Adv. Mater.* **2012**, *24*, 1961.
[54] H. J. Zhao, J. Íñiguez, W. Ren, X. M. Chen, L. Bellaiche, *Phys. Rev. B.* **2014**, *89*, 174101.